Time-Dependent Nonlinearity of Compression Softening in Concrete

Khaled Farouk El-Kashif[1] and Koichi Maekawa[2]

Received 29 September 2003, accepted 19 February 2004

Abstract

As nonlinear post-peak mechanics is time dependent in nature and the transient process of collapse is influenced by loading rates, post-peak analyses have to be conducted considering softened structural concrete under varying rates of straining. To meet this challenge, a new time-dependent constitutive model, which encompasses both near- and post-peak regions in concrete compression, is proposed. Towards better evaluation of structural collapse under extreme loads, a coupled plastic-damaging law is presented. For the purpose of identifying evolution laws of plasticity and continuum damage, experimental investigation into rate-dependent nonlinearity was performed under different levels of lateral confinement. The plastic and damage evolutions were formulated with respect to paths of intrinsic stress intensity of damage continua and time. The combined law of short-term elasto-plastic and fracture successfully convey nonlinear creep deformation and rate dependent strength, as well as delayed creep rupture of material instability.

1. Introduction

In the scheme of performance-based design, demands for the simulation of structural collapse are increasing for a sounder description of global safety factors. Currently, research efforts are being made in the area of post-peak analyses of concrete structures, and concrete nonlinearity of softened compression is regarded as one of the key issues. Here, time-dependency turns out to be predominant when stress level exceeds 70% of the specific uniaxial strength of concrete and instability may occur in the form of creep rupture within a shorter period of stressing (Rusch 1960). This tendency is greatly accelerated beyond the peak. Current advanced computational mechanics enables us to simulate capacity as well as transient states until complete collapse. Thus enhanced material modeling directly contributes to the upgrading of post-peak analyses and their reliability.

As loading rates of static experiments in laboratories greatly differ from those of dynamic experiments in the case of earthquakes, Okamura *et al*. took into account time-dependency in their static/dynamic nonlinear structural analyses (Maekawa *et al*. 2003) under higher stresses by simply factorizing the plastic evolution law for concrete. As ultimate limit states of reinforced concrete are comparatively less time-dependent in practice, simplified approaches have been practically acceptable. As far as post-peak analysis is concerned, however, the rate effect is becoming significant in nature and the authors empathize that explicit consideration of time-dependent nonlinearity of compression softening is required in collapse analyses.

Here, it should be noted that the structural concrete of collapsing structures undergoes varying strain or stress rates. Even if the external displacement rate were kept constant, quite a high strain rate would be provoked around localized zones of deformation. On the contrary, the neighboring volumes next to the localized zone reveal rapid recovery of deformation. Thus, the scope of research has to be the short-term time-dependency on both loading and unloading paths. This implies that the stress-strain model under constant rate of loading cannot meet the requirement for collapse analysis. To meet this challenge, a new versatile time-dependent constitutive model, which encompasses both near- and post-peak regions in concrete compression, is proposed in this paper.

Tabata and Song *et al*. investigated combined creep-relaxation hysteresis close to the uniaxial strength and extracted both short-term plastic and damaging evolutions (Tabata *et al*. 1984, Song *et al*. 1991). They concluded that the combined elasto-plastic and damaging concept could be applied to pre- and post-peak time-dependent mechanics (Maekawa *et al*. 1984). This paper basically goes along this mechanics and further extends the applicability to generic 3D confined conditions to fulfill the requirement of the post-peak analyses. Concrete is a heterogeneous cohesive-frictional material that is highly pressure-sensitive and in which compressive stress transfer is accomplished to a great extent by frictional forces after the peak (Pallewatta *et al*. 1995, Sheikh 1982, Scott *et al*. 1982). There are two well-known facts, namely the fact that confinement is very effective for improving post-peak responses, and the fact that time-dependency becomes significant in the post-peak region. However, the lack of combined knowledge does not enable us to proceed to post-peak analyses in time domains. In this paper, the authors primarily intend to formulate the one-dimensional high rate transient nonlinearity of concrete compression. Ap-

[1]Post Doctoral Fellow, Department of Civil Engineering University of Tokyo, Japan
[2]Professor, Department of Civil Engineering, University of Tokyo, Japan
Email: maekawa@concrete.t.u-tokyo.ac.jp

plication for post-peak analysis is to be done in a separate study.

2. Experiment

The experimental works described in the following sections were conducted on the basis of uniaxial compressive loading to concrete cylinders 10 cm in diameter and 20 cm in height. The specimens were cured under the standardized condition for 28 days and allowed to be exposed to indoor ambient conditions for an additional period of two weeks. The material composition that was used is shown in **Table 1**. Various confining pressures were applied by using steel rings embedded in advance. The specimens and their details are shown **Fig. 1** and tabulated in **Table 2** and **Table 3**. Axial capacity of concrete with lateral confinement is spatially averaged over the whole section (Irawan *et al*. 1994). As a circular section was used, local stress over a section can be assumed to be uniform due to axial symmetry. The applied lateral stress can be calculated according to $\frac{1}{2}\rho_s f_y$ (Mander *et al*. 1988) by assuming full yield of lateral steel close to and after the peak capacity.

The main measurements were axial mean stress and strain of cylindrical specimens. Axial deformation was measured by using displacement transducers. The measured strain is the special averaged strain over the length of the specimens. Thus, the compressive localized zone is included inside this characteristic length. To produce uniformity of strain field, proper bedding between specimen ends and machine platens was aimed for placing a rapid hardening cement grout layer. Correct concentricity was assured by monitoring displacement transducers whose reading was settled within 10% variation at three points. The test setup is shown in **Fig. 2**.

The elasto-plastic and damage model as summarized in **Fig. 3** is selected as the mechanical basis for expressing nonlinearity. Within this scheme, the evolved plastic rate of deformation was formulated in terms of elastic strain, which represents the intrinsic stress intensity of the damaging continuum (Maekawa *et al*. 2003). Further, reduced elastic stiffness, which can be seen in unloading paths and described by a fracture parameter, was also devised in terms of intrinsic elasticity. Damage is conceptually defined as a loss of parallel components (see **Fig. 4**), and the fracture parameter indicates the ratio of working elements. In this study, the authors intend to incorporate the time-dependent plastic rate and supplementary damage with instantaneous strain path depend-

Table 1 Material composition for 1m^3.

Material type	Water cement ratio	Cement (kg/m^3)	Sand (kg/m^3)	Gravel (kg/m^3)	Admixture Agent (mm^3/m^3)
Normal concrete	0.5	352	866	890	440

Table 2 Lateral steel arrangement.

Lateral Steel Arrangement	Spacing (mm)	Yield Strength (MPa)	D1(mm) (inner)	D2(mm) (outer)	Lateral Stress (MPa)
Not Used	-	-	-	-	-
15mm height	50	350	90	99	9.0
10mm height	50	350	90	99	6.0
10mm height	50	350	94	99	3.3

Table 3 Tested condition of specimens.

Specimen	Concrete Compressive Strength (MPa)	Age at Test (Day)	Lateral Pressure (MPa)
A-0.0-a	3.30	38	0.0
A-0.0-b	3.45	40	0.0
A-0.0-c	3.80	42	0.0
A-0.0-d	3.45	40	0.0
A-0.0-e	3.25	35	0.0
A-0.0-f	3.15	46	0.0
A-3.3-a	31.0	40	3.3
A-3.3-b	30.0	42	3.3
A-6.0-a	32.20	47	6.0
A-6.0-b	34.0	52	6.0
A-9.0-a	32.3	55	9.0
A-9.0-b	29.3	51	9.0

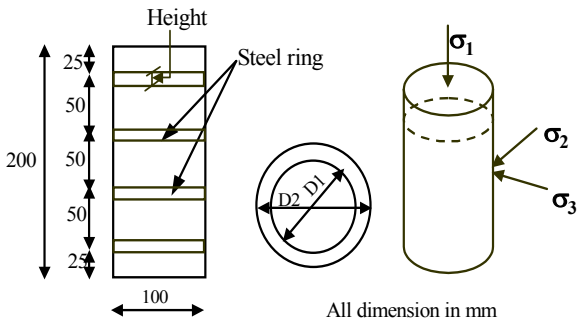

Fig. 1 Laterally confined specimen details.

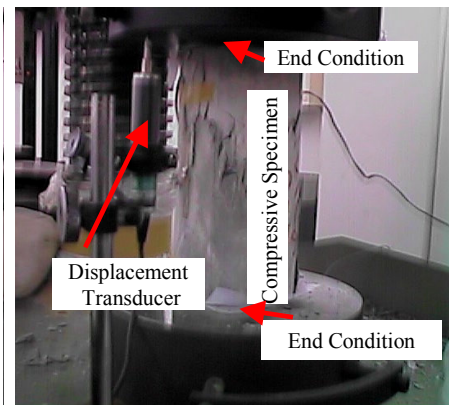

Fig. 2 Test setup and displacement measurement.

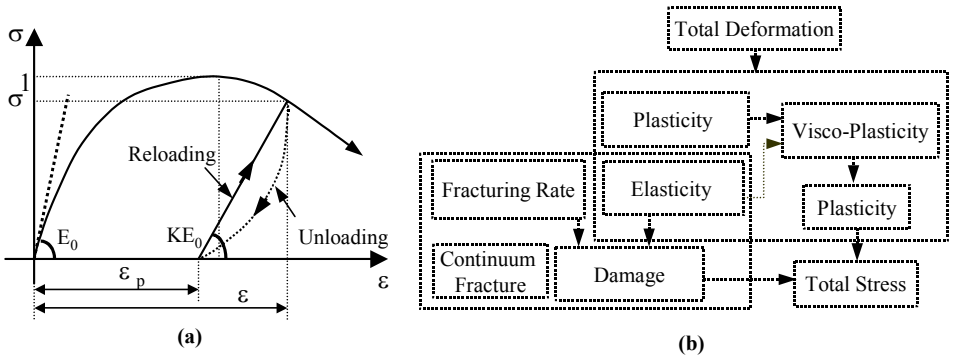

Fig. 3 Concept elasto-plastic and damaging model: (a) definition (b) scheme of formulation.

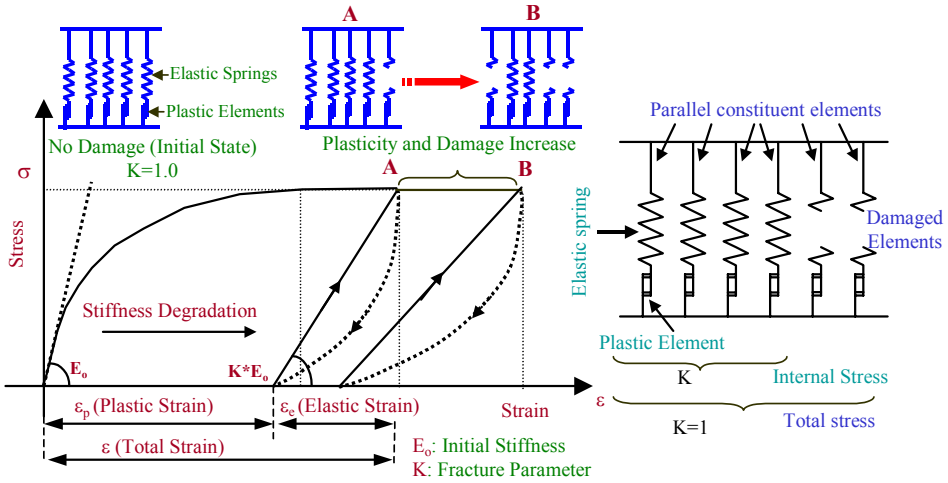

Fig. 4 Schematic representation of elasto-plastic and damage concept.

ent nonlinearity as stated before.

Elasto-plastic and damaging concept is schematically expressed as assembled parallel elements consisting of elasto-plastic sliders. Here, broken elements are represented as damaged ones in past mechanics, and the total stress is taken as an integral of internal stresses of remaining elements. According to the analogy shown in **Fig. 4**, the intrinsic stress intensity applied to each non-damaged component is directly proportional to elastic strain. Then, time-elasticity path is thought to be a logical operator to rule both plastic and damaging growths.

Maekawa *et al*. presented evolution laws of plasticity and damage with respect to elastic strain increment under high rate loading (Maekawa *et al*. 2003). In order to further obtain their time-dependency, the authors applied three patterns of total stress-strain hysteresis in experiment as shown in **Fig. 5**, where A and B denote different mechanical states specified on stress-strain space. Rapid stress release from these two states may earn plastic strain increment and variation of the fracture parameter. The elastic strain also varies slightly from state A to state B even if the total stress is kept constant. Here, the average elastic strain between state A and state B can be thought to represent the average internal stress intensity of active components during this transient condition. Thus, we can have a set of evolution ($d\varepsilon_p/dt$, dK/dt) by the form of finite time-difference and corresponding averaged state variables (ε_p, K, ε_e) from an experiment where total compression is sustained.

Under the relaxation path for keeping the total strain constant, we may get hold of evolved transient nonlinearity and subsequent state variables in the same manner. In this study, creep and relaxation paths were applied to concrete with different magnitudes of confinement. Furthermore, the authors included their combinations, in which total strain occurs but the total stress is softened in post-peak region as shown in **Fig. 5**. If there would be a unique relation between nonlinearity rates and the state variables in spite of various time-stress-strain histories, it can be a rate-type constitutive law of generality. In this paper, attention is mainly directed to this distinctiveness.

Figure 6a shows the extracted rates of plasticity and fracturing ($d\varepsilon_p/dt$, dK/dt) from various loading paths under different intrinsic stress/strain levels of (ε_p, K, ε_e) as shown in **Fig. 14** under unconfined compression. It is

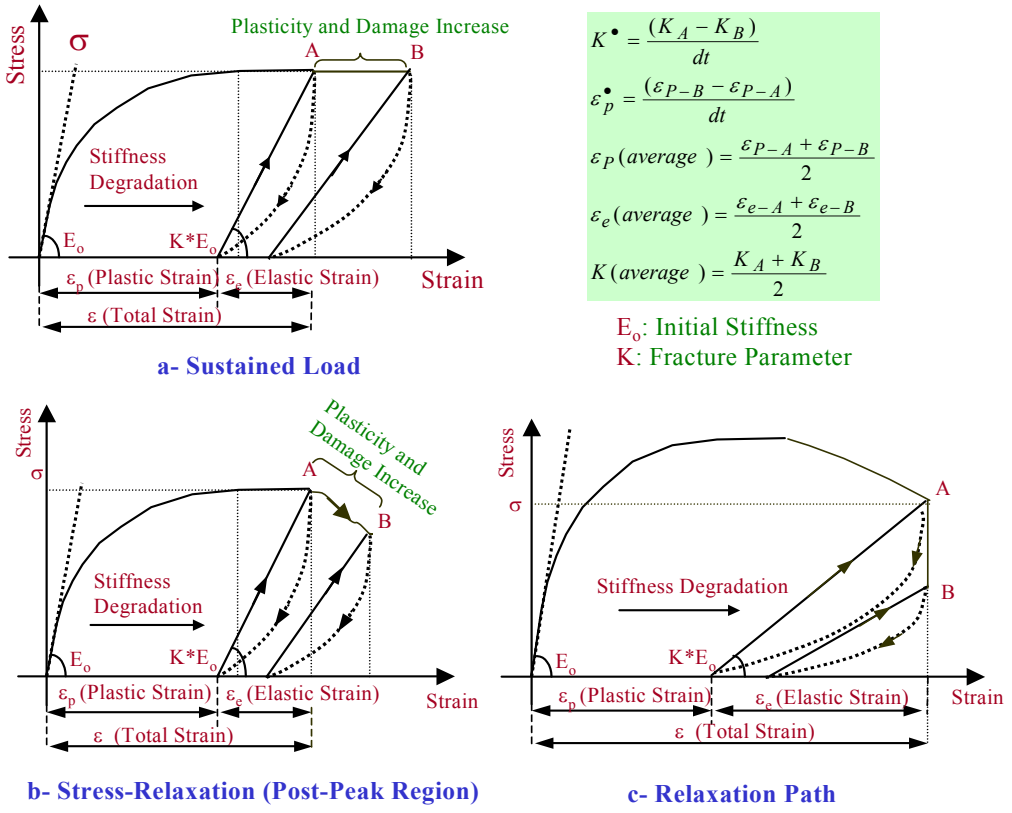

Fig. 5 Extraction of time-dependent evolution of plasticity and damaging.

clearly shown that the plastic rate under the similar elastic strain levels is sharply reduced when the absolute plastic strain evolves, and that the plastic rate depends to a high degree on the magnitude of elastic strain. Just before creep failure, an increase in progressive total strain was experienced. Herein, the elasticity was simultaneously amplified due to simultaneously evolving damage even though the total stress level was kept unchanged. This trend is qualitatively similar to long-term creep under lower stress states where continuum damage is hardly seen. However, the observed transient plastic flow is thought to be caused by shear slides along micro-cracks (Maekawa *et al*. 2003), and its rate is significantly higher than the creep flow rate associated with CSH gel grains and moisture dynamics under lower stress states. The larger elasticity is developed, the higher the rate of plasticity that is produced. This is also analogous to the long-term creep properties of concrete in nature but rather nonlinear with respect to the magnitude of stress or elastic strains. These experimentally observed behaviors do not contradict the elasto-plastic and damage concepts.

The damage evolution is not seen under low stress states less than 30% of the specific uniaxial compressive strength, but it becomes significant under near or post-peak conditions. The fracturing rate is rapidly reduced when fracture itself occurs under the similar magnitude of elasticity that represents the internal stress intensity. Damage (reduction of elasticity) is attributed to growth of distributed micro cracks associated with deteriorated capacity of elastic shear strain energy (Maekawa *et al*. 2003). As a matter of fact, it takes time for crack propagation in a finite domain, and it can be seen in **Fig. 6a** that the rate of fracturing is dependent on internal stress intensity in pre and post-peak states.

The extracted data from experiments of confined concrete (see **Fig. 15** to **Fig. 17**) was processed and summarized as shown in **Fig. 6b**. As all lateral steel rings yield just before and after the peak strength of each specimen when nonlinearity evolves, lateral confining stress denoted by σ_l (see section **2.1**) is computed by solving lateral equilibrium as shown in **Fig. 6b**. On unloading and reloading paths, lateral steel rings return to elasticity. Here, a reduced amount of nonlinear evolution was observed. It is recognized that the damaging rate is reduced in absolute terms according to the increase in confining pressure. In physical terms, this means that higher confinement stabilizes transitional damaging of concrete and seems reasonable for composite frictional materials. Although the effect of confinement is seen in time-dependent plasticity, it is comparatively small. This means that the growth of plastic deformation is not well restrained by confinement when the stress is applied near the capacity, or strain crosses the capacity threshold. In the following chapter, nonlinear evolution laws will be formulated for computational mechanics.

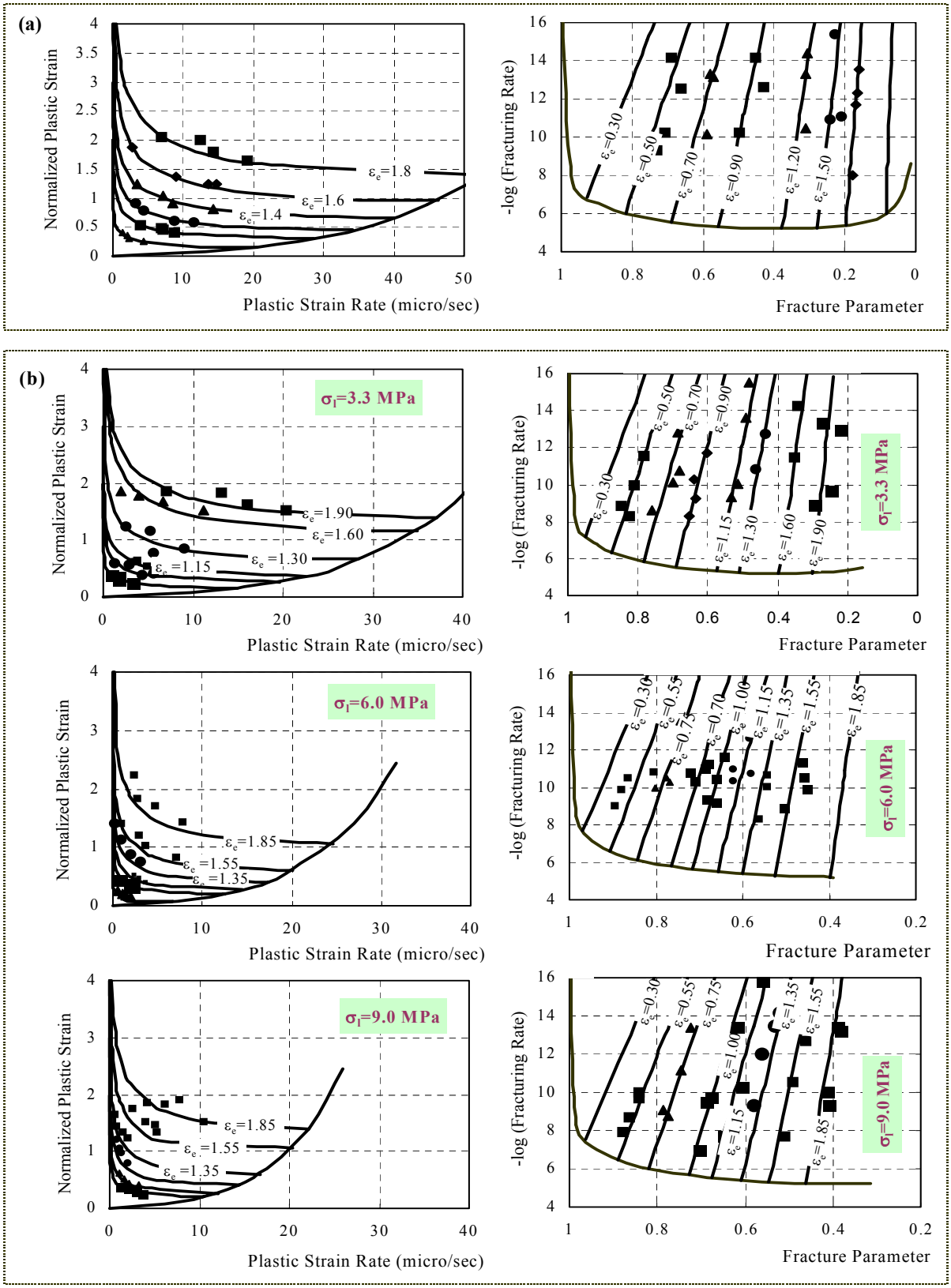

Fig. 6 Extracted plastic and damaging rates: (a) unconfined, (b) confined concrete (Dot points = experimental data, solid lines = analytical model).

3. Model Formulation

3.1 Potential term of nonlinearity

The basic constitutive equations to express the elasto-plastic and damaging concepts (see **Fig. 4**) and the general Taylor's series of state variables (plastic strain and fracture parameter) can be reduced to,

$$\varepsilon = \varepsilon_e + \varepsilon_p\ ,\quad \sigma = E_o \varepsilon_e K \tag{1}$$

$$d\varepsilon_p = \left(\frac{\partial \varepsilon_p}{\partial t}\right) \mathrm{d}t + \left(\frac{\partial \varepsilon_p}{\partial \varepsilon_e}\right) \mathrm{d}\varepsilon_e$$

$$dK = \left(\frac{\partial K}{\partial t}\right) \mathrm{d}t + \left(\frac{\partial K}{\partial \varepsilon_e}\right) \mathrm{d}\varepsilon_e \tag{2}$$

where K = fracture parameter, ε_e = elastic strain, ε_p = plastic strain, σ = stress, t = time and E_o = initial elastic modulus.

For simplicity of formulation, the above stress and strain are defined as normalized stress and strain using the specific uniaxial compressive strength and the corresponding peak strain, respectively. Similar to the theory of plasticity, it was experimentally established that plastic and damage potentials (F_p, F_k) exist and create envelope surface described by (F_p, F_k)=0, where the derivatives with respect to the elastic strain in Eq. 2 reveal non-zero. As nonlinearity also occurs by satisfying conditions dF_p=0 and dF_k=0, we have,

$$\left(\frac{\partial \varepsilon_p}{\partial \varepsilon_e}\right) = 0 \quad \text{when } \mathrm{F_p} > 0$$

$$\left(\frac{\partial \varepsilon_p}{\partial \varepsilon_e}\right) = -(\partial F_p / \partial \varepsilon_e)/(\partial F_p / \partial \varepsilon_p) \quad \text{when } \mathrm{F_p} = 0 \tag{3}$$

$$\left(\frac{\partial K}{\partial \varepsilon_e}\right) = 0 \quad \text{when } \mathrm{F_k} > 0$$

$$\left(\frac{\partial K}{\partial \varepsilon_e}\right) = -(\partial F_k / \partial \varepsilon_e)/(\partial F_k / \partial K) \quad \text{when } \mathrm{F_k} = 0 \tag{4}$$

The potential functions were experimentally formulated for unconfined normal strength concrete (Maekawa *et al*. 2003) as,

$$F_\mathrm{p} = \varepsilon_p - 0.038\left(\exp\left(\frac{\varepsilon_e}{0.55}\right) - 1\right) \tag{5}$$

$$F_k = K - \exp\{-0.73\beta(1 - \exp(-1.25\beta))\}$$

$$\beta = -\frac{1}{0.35}\left(\ln\left(1 - \frac{7\varepsilon_{ec}}{20}\right)\right) \tag{6}$$

where $\varepsilon_{ec} = \varepsilon_e$ in case of the unconfined condition.

Figure 7a and **Fig. 8a** illustrate the plastic and fracturing potentials, respectively (Maekawa *et al*. 2003), derived from experiments under higher loading rates. Here, the time dependent plasticity and fracture are thought to be negligibly small.

It is experimentally known that the confining pressure elevates the uniaxial strength (Richart *et al*. 1928) and ductility. This effect was successfully explained only by the suppressed damage evolution denoted by F_k as illustrated in **Fig. 8d**. It was also revealed that, on the contrary, plastic evolution of concrete is not affected by confinement (Maekawa *et al*. 2003). Here, the authors extend the original damage potential of concrete (Eq. 6) to more generic states under lateral confinement by using confinement parameter γ defined by Eq. 7. The unconfined condition corresponds to unity of γ and higher confinement reduces this index to null as an extreme confinement. The following strain modification factor for Eq. 6 is presented so that total stress-strain relation matches the reality of confined concrete as,

$$\varepsilon_{ec} = \psi \cdot \varepsilon_e, \quad \psi = \gamma^a, \quad \gamma = \frac{f_c}{f_\mathrm{c} + 4 \cdot \sigma_1} \tag{7}$$

$$\mathrm{a} = Y^{0.4(1 - \exp(-5Y))}, \quad Y = \frac{\varepsilon_e}{3.25 - 2.65\gamma} \tag{8}$$

where, f_c = uniaxial compressive strength, σ_1 = lateral confining pressure. In the following section, formulation of nonlinear derivatives with respect to time will be discussed.

3.2 Plastic rate function

Figure 7a schematically shows the instantaneous plasticity envelope (F_p=0) and the rate of plasticity on the (ε_e, ε_p) plane. It is natural to assume that the rate of plasticity exhibits the maximum on the instantaneous plastic potential envelope, and that the specific plastic rate on the envelope increases in accordance with the magnitude of elasticity as illustrated in **Fig. 7b**. As described in section 2.5 and shown in **Fig. 7a**, the rate of plasticity decays as the state of active elasto-plastic components represented by (ε_e, ε_p) moves away from the envelope. Thus, the authors propose the following mathematical form,

$$\frac{\partial \varepsilon_p}{\partial t} = \phi\left(\frac{\partial \varepsilon_p}{\partial t}\right)_\mathrm{b}, \left(\frac{\partial \varepsilon_p}{\partial t}\right)_b = 0.034\left(\exp\left(\frac{\varepsilon_{ep}}{4}\right) - 1\right) \tag{9a}$$

$$\phi = \exp\left(-6\left(\frac{F_p^{0.6}}{\varepsilon_e^{1.2}}\right)\right), \qquad \varepsilon_{ep} = \gamma\, \varepsilon_e \tag{9b}$$

where $(\partial\varepsilon_p/\partial t)_b$ means the referential rate defined on the plastic potential envelope, ϕ indicates the reduction factor in terms of plastic evolution as shown in **Fig. 7c** and ε_{ep} means the equivalent elastic strain corresponding to the confining pressure level.

The values computed by Eq. 9 are overlaid on **Fig. 6a**

and **Fig. 6b** for both plain and confined concrete. The plastic rate function can be uniquely specified by the elastic strain to represent the intrinsic stress applied to the parallel components. If the total stress are used for the plastic rate function, a unique relation of $d\varepsilon_p/dt$ and σ cannot be found since at least two plastic strains may exist in the pre- and post-peak regions corresponding to the total stress.

3.3 Damaging rate function

Figure 8a indicates the tendency of the fracturing rate on the (ε_e, K) space. Similar to the case of plasticity, the fracturing rate decreases according to the continuum damage evolution under sustained elastic strains. For rational formulation, it is meaningful to clarify the physical image of continuum fracturing represented by K. Song introduced fictitious non-uniformity of parallel elasto-plastic components as a source of damage (Song *et al*. 1991) and explained the instantaneous evolution of fracturing. This concept is implemented with regard to the potential term in Eq. 4, but it does not conceptually cover the delayed fracturing term denoted by d*K*/dt.

Delayed fracturing is thought to be associated with micro-crack propagation. Newly created micro-cracks can develop just inside remaining non-damaged volume that is denoted by *K*. Thus, even though the probability of delayed fracturing would be common among individual components, the averaged fracturing rate of the assembly of remaining components will be proportional to *K*. In fact, the fracturing rate shall be null when the fracture parameter converges to zero as shown in **Fig. 8b**. Then, the following formulae based upon this imaginary micro-fracture are introduced as,

$$\frac{\partial \mathrm{K}}{\partial \mathrm{t}} = \left(\frac{\partial \mathrm{K}}{\partial \mathrm{t}}\right)_{\mathrm{b}} \exp\left(\xi\left(\frac{K}{K - F_k} - 1\right)\right)$$

$$\xi = 45\left[\psi - 0.5(1 - \exp(-5\varepsilon_e))\right] \tag{10a}$$

$$\left(\frac{\partial K}{\partial t}\right)_{\mathrm{b}} = \left(\frac{\partial K}{\partial t}\right)_{n} (K - F_k)$$

$$\left(\frac{\partial K}{\partial t}\right)_{n} = 0.015 \cdot \log(K - F_k) \tag{10b}$$

where, $(dK/dt)_b$ represents the referential fracturing rate on the envelope (F_k=0) on which instantaneous fracturing may occur with respect to the increment of elasticity.

In order to formulate $(dK/dt)_b$, the intrinsic fracturing rate to indicate the delayed evolution of micro-crack per unit active volume is given in the same manner as plasticity. As stated above, this rate is factored by the fracture parameter (K- F_k) in order to consider the remaining volume where new micro-defects can develop. As the potential F_k is a function of confinement, $(dK/dt)_b$ is also associated with the intensity of confinement as dis-

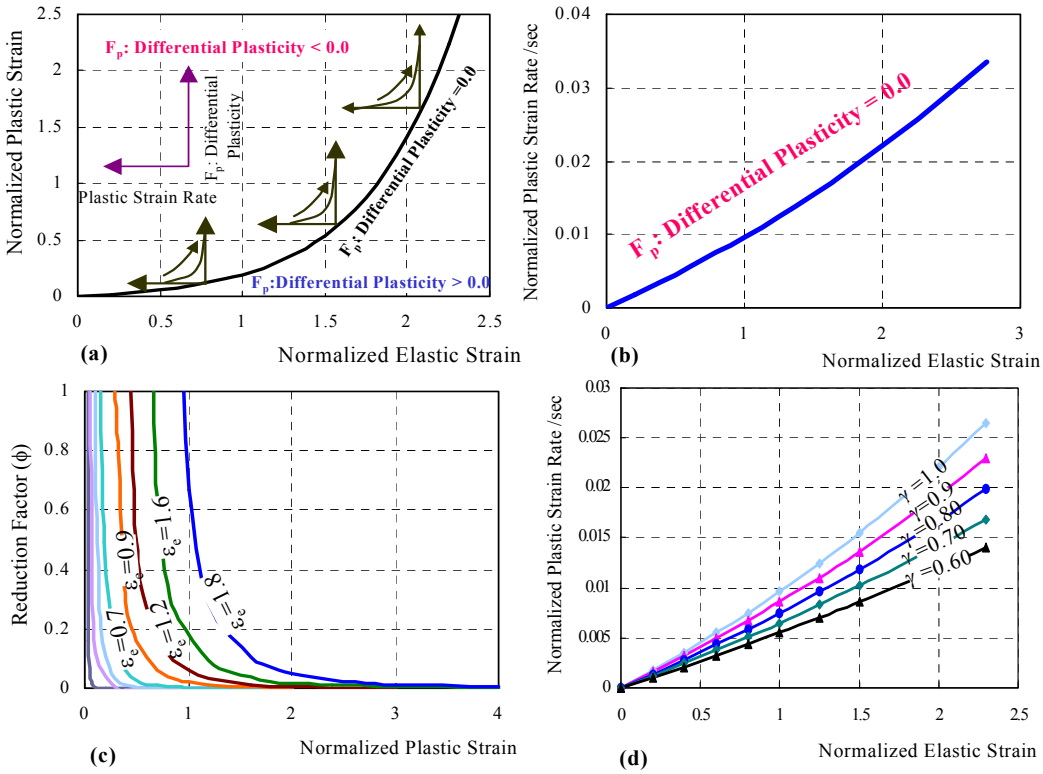

Fig. 7 Formulation scheme of time-dependent plasticity: (a) sensitivity of updated plasticity and elasticity on plastic flow rate, (b) flow rate on potential envelope, (c) decay of flow rate, (d) effect of confinement on flow rate on potential envelope.

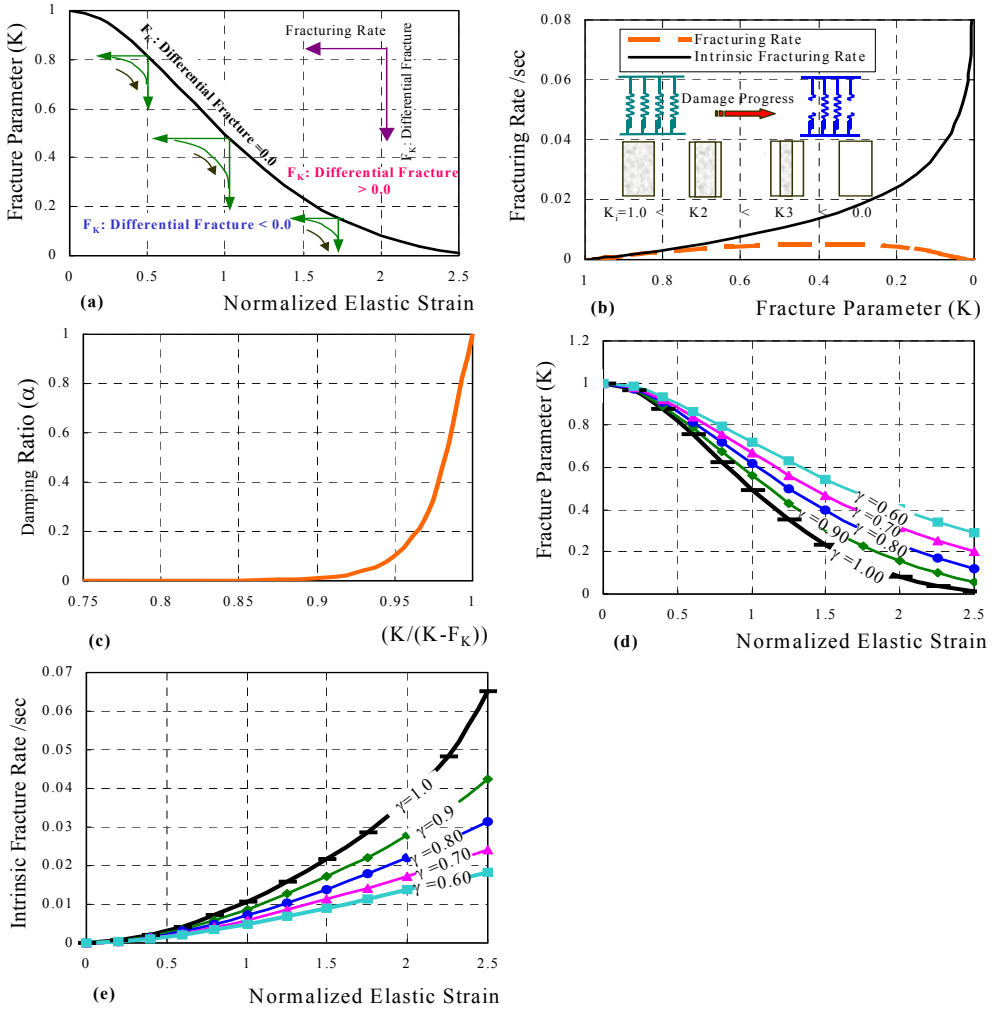

Fig. 8 Formulation scheme of time-dependent damage: (a) sensitivity of updated damage and elasticity on damage evolution, (b) damaging rate on potential envelope, (c) decay of damaging, (d) effect of confinement on damage evolution on potential envelope, (e) effect of confinement on damaging rate on potential envelope.

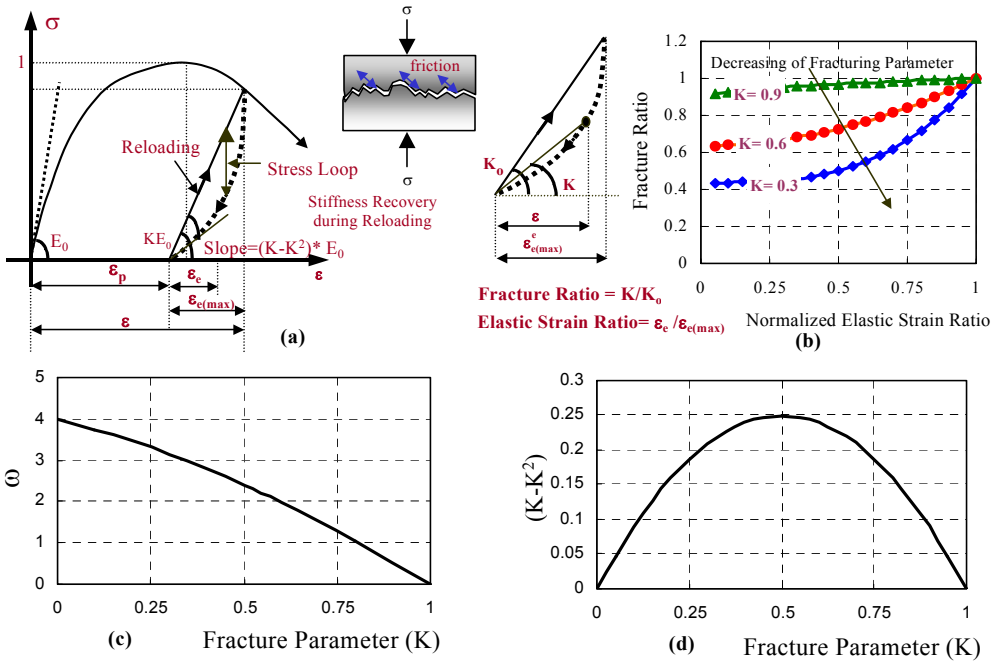

Fig. 9 Formulation scheme of internal loop: (a) nonlinear stress loop, (b) secant stiffness ratio, (c) nonlinear order in terms of elastic strain, (d) stiffness ratio of internal stress loop (α in Eq. 12).

cussed in section 2.5 and shown in **Fig. 8e**. The computed rates are shown with experiments in **Fig. 6a** and **Fig. 6b**.

3.4 Computational model for internal loop

The simple combination of elasto-plastic and damage results in partial linearity in unloading-reloading paths without any hysteresis loop. Although this simplicity does not reflect the reality as shown in **Fig. 9**, it is acceptable for structural analysis to verify some limit states of capacity. For seismic analysis, however, the partial linearity of stress-strain relation leads to lower energy absorption under repeated cycles of loads. In the case of post-peak analyses, tangential unloading stiffness at high stress states substantially affects the computed intensity of strain localization. Thus, this section focuses on the formulation of hysteretic nonlinearity in unloading/reloading paths where instantaneous plasticity and damaging do not occur.

Figure 9 shows the transition of secant stiffness normalized by the fracture parameter for different damage levels and confinement. Generally, the unloading loop tends to deviate from the linear line specified by the fracture parameter according to damage evolution (0.5<K<1.0). This deviation is suppressed by the presence of lateral confinement. By referring to the computational model for cracked concrete, the authors incorporate the following fictitious loop stress into Eq. 1 as,

$$\sigma = E_o \mathrm{K} \varepsilon_{\mathrm{e}} + \sigma_{\mathrm{loop}}, \quad \sigma_{\mathrm{loop}} = E_{loop} \varepsilon_{\mathrm{e}} \tag{12a}$$

$$E_{loop} = -\alpha \cdot E_o \left(1 - \left(\frac{\varepsilon_e}{\varepsilon_{e(\max)}} \right)^{\omega} \right) \tag{12b}$$

$$\omega = 4 - 2.4K - 1.6K^2, \qquad \alpha = (K - K^2) \tag{12c}$$

where the value of α is defined as the stiffness ratio of internal loop at zero stress as shown in **Fig. 9**. The applicability of Eq. 12 to unloading paths can be seen in **Fig. 10**. The reloading paths are assumed to linearly come up to the past maximum elastic strain denoted by $\varepsilon_{e(\max)}$.

3.5 Extreme boundary of fracture

Concrete finally comes near to assembly of aggregates which are mutually broken away and cementing performance of paste matrix is lost due to full micro-crack propagation. But, this extreme state still remain residual stress with frictional nature when lateral confinement is maintained as shown in **Fig. 11**. The residual capacity denoted by σ_{lim} is thought equilibrated with the lateral confining pressure and frictional stress transfer along the shear band of aggregates assembly. As the fracture parameter corresponding to this extreme state of damage is thought to be lower bound of the confined concrete, we have,

$$K_{\mathrm{lim}} = \frac{\sigma_{\mathrm{lim}}}{2E_o \varepsilon_{e\,\mathrm{lim}}} \tag{13a}$$

$$\sigma_{\mathrm{lim}} = \sigma_l \frac{\sin(\theta) - \mu \cdot \cos(\theta)}{\cos(\theta) + \mu \cdot \sin(\theta)} \tag{13b}$$

$$\theta = \frac{\pi}{4}\left(2 - e^{(-\sigma_l / 6.5)}\right), \quad \varepsilon_{\mathrm{elim}} = 2.85.(\gamma^{-0.5})$$

where, μ= coefficient of friction for concrete and it equals to 0.6, σ_l = lateral confining stress in MPa, θ = directional angle of shear fracturing band and obtained by equilibrium conditions in terms of confinement and $\varepsilon_{\mathrm{elim}}$ which is defined as normalized elastic strain corresponding to fracture limit. It is empirically obtained by Eq. 13b.

It should be noted that this extreme boundary of fracture parameter does not play any substantial role in computed results of structural concrete but numerically avoid accidental crush or divergence of nonlinear iterative computation.

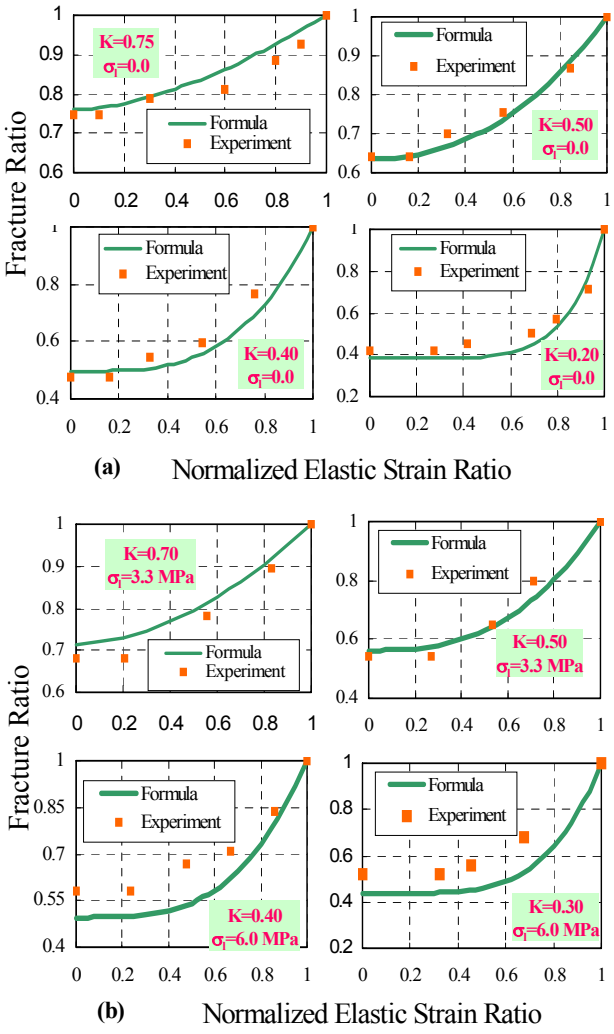

Fig. 10 Secant stiffness and elastic strain relation:(a) unconfined (b) confined concrete.

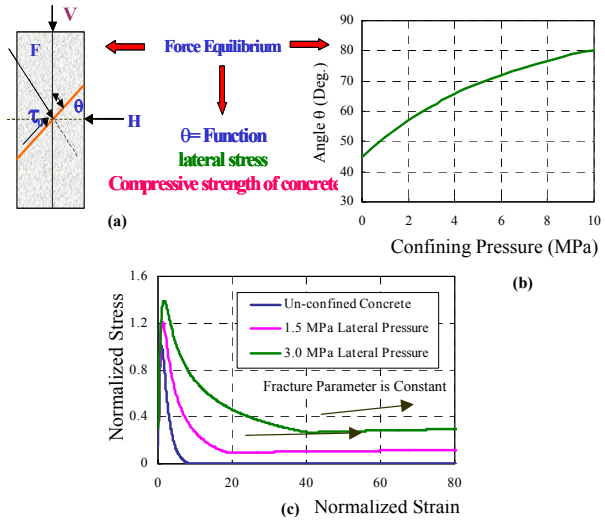

Fig. 11 Damage limit state of confined concrete.

4. Model verification

The differential form of total stress strain relation is derived by simultaneously solving equations (1)-(13), and the total stress/strain can be integrated under any strain/stress history. Here, the experimental verification is performed under different strain or stress histories for pre- and post-peak regions. It is clearly stated that the proposed modeling is applicable to concrete whose referential volume size is approximately 20-30 cm. This size is equivalent to the size of standardized cylindrical specimens for strength and Niwa reported that the actually produced size of compression localization in RC structures is almost 20-30 cm (Lettsrisakulrat *et al.* 2000). For consistency in experimental verification, the similar sized volume, on which the space-averaged strains are defined, is selected in this chapter. When the proposed modeling would be used for finite elements whose size much differs from the referential size of 20-30cm, space-averaged constitutive model shall be adjusted so as to have consistency in terms of fracture energy or ultimate limit displacement in shear band.

4.1 Creep rupture

It is known that delayed creep failure may take place in compression provided that the applied sustained stresses exceeds approximately 70% of uniaxial compressive strength of concrete. **Figure 12** shows the computed short-term creep under sustained stresses and experimental facts of unconfined concrete (specimen size: 10 cm diameter and 30 cm height) reported by Rusch (1960). The creep rupture is computationally distinguished as a singular point where the rates of total and elastic strains attain infinite but the plastic rate is negligibly small. It means that the elasticity at this singular point lies on the damaging envelope on the (ε_e, K)-plane mathematically indicated by $F_k(\varepsilon_e, K)=0$, and instantaneous evolution of damage occurs at the same time. Here, the increase in intrinsic stress (represented by elastic strain) over the living elements is counterbalanced by the progressive fracturing of the continuum.

The ultimate strain and the elapsed time until creep rupture are well simulated and the sensitivity of stress level is adequately predicted by the model. The computed elapsed time until the creep rupture is influenced mainly by the model of time-dependent damage, and the computed ultimate creep strain is largely affected by the formulated rate of plastic flow. Both models are expected to be validated.

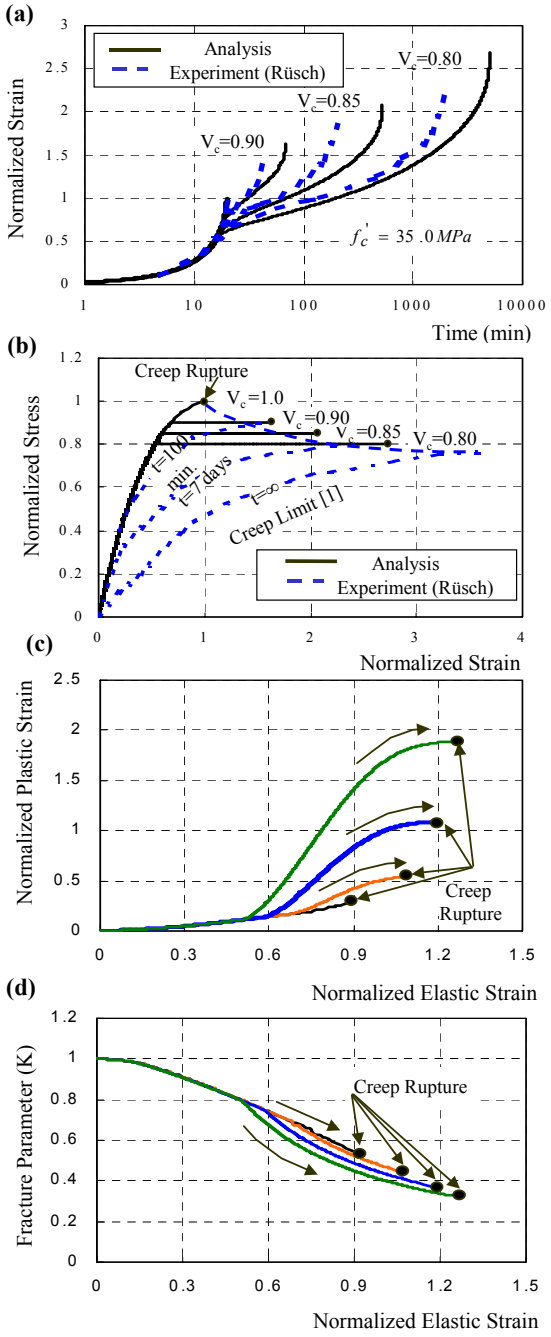

Fig. 12 Simulation of creep rupture: (a) creep strain in progress, (b) ultimate rupture strain and elapsed time, (c) elasto-plastic paths, (d) elasto-damaging paths.

4.2 Monotonic stress-strain relation under constant strain rate

It is well known that the stress-strain relation is not unique but strain rate dependent. As a matter of fact, the stress or strain rate is clearly specified in the standardized test for compressive strength of concrete. **Figure 13** shows the computed stress-strain relation under different rates of strain and comparison with experimental results as reported by Rusch (1960). Here, the strain is normalized by the peak strain corresponding to the specified compressive strength as stated above. It is clearly found that the computed peak strength and its strain depend on loading rates. When the lower rate of strain is assumed, the apparent strength decreases and the peak strain increases. This behavioral simulation quantitatively coincides with the reality.

Figure 13 also indicates the internal variables of this simulation. The lower rate of loading causes large plasticity to a great extent and damaging occurs. Thus, the strength decay under lower rates of loading is mainly attributed to time-dependent damage, and the apparent reduced stiffness is brought about by progressive time-dependent plasticity. Reasonable agreement is seen in these loading paths. The tangential stiffness on the descending portion of stress-strain relations has much to do with computed results of compressive localization. The softened compressive stiffness can be recognized as time-dependent and well simulated.

4.3 Generalized stress-strain paths

Figure 14 shows the short-term nonlinear creep paths close to and beyond the uniaxial capacity of unconfined concrete. The greater progress of the total strain is seen especially in the post-peak zone but comparatively smaller evolution of plasticity can be observed. The unloading stiffness varies over time and it drastically drops in the softening condition. It must be noted that time dependent plasticity and fracturing continue to occur even though the unloading paths are enforced to concrete and this leads to some nonlinearity shown in cyclic hysteresis under highly damaged conditions.

The relaxation paths in pre and post-peak zones were also focused for validation of modeling as shown in **Fig. 14**. The computed and experimentally obtained elapsed times of stress relaxation are compared at each total strain level and good agreement is observed. The generalized loading paths of combined creep and relaxation are also checked in **Fig. 14**. The simultaneous evolution of plasticity and damaging can be seen in the experimentally obtained stress strain relation and the computational model fairly predicts this coupled behavior.

The experimental verification is performed for different levels of confining pressure. **Figure 15** shows the influence of confining pressure on the overall stress-strain relation. The strength gain by confinement (3.3MPa) can be well simulated. It is rooted in suppressed evolution of damaging. Furthermore, the strain kinematics under higher stresses can be stabilized as shown in **Fig. 15a**. Under the confined situation, stress can be well maintained for softened concrete even after the peak capacity, and the stabilized rate of creep deformation can be simulated as shown in **Fig. 15b**. However, when the plastic and damage nonlinearity is experienced first, singularity of creep rupture may occur in the post-peak softening in both analyses and experiments.

The nonlinear creep deformation under sustained stresses is shown in **Fig. 16** and **Fig. 17** for more highly confined concrete. The nonlinear creep strains were measured and simulated before and after the peak capacity. Before the peak, the creep strain rate is greatly restricted by applying higher confinement when we compare these figures under the same stresses. But when the applied stress is set close to the elevated capacity by confinement, the creep rate is not small in practice. According to the confinement, unloading- reloading stiffness hardly decreases and the mechanical behavior looks like perfect elasto-plasticity. This means that damage evolution is effectively restrained by 3D confinement. As a result, we have a low rate of time-

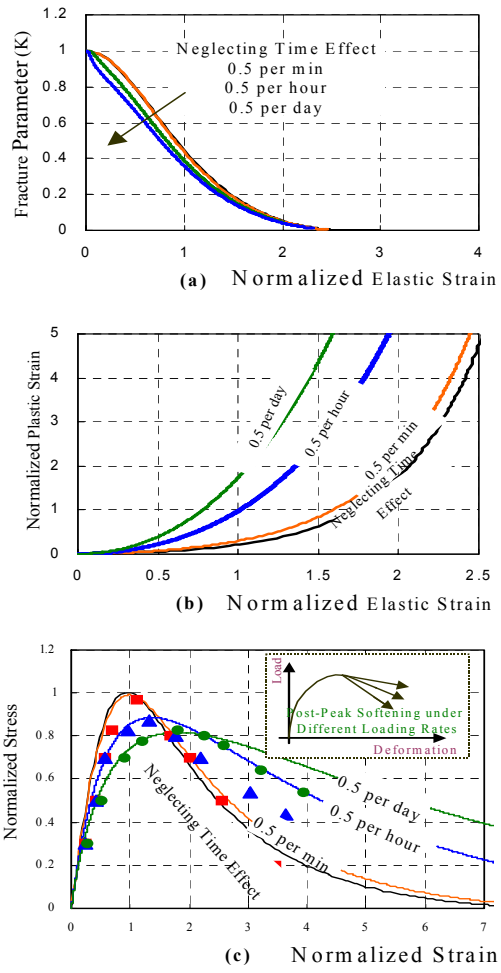

Fig. 13 Stress-strain relation under constant strain rates: (a) elasto-plastic paths, (b) elasto-damaging paths, (c) normalized stress versus strain relation (dot points = experiments, lines = analytical model).

dependent deformation even in the post-peak conditions. The coupled elasto-plastic and fracturing model reasonably represents the behavioral simulation of materials with higher reliability.

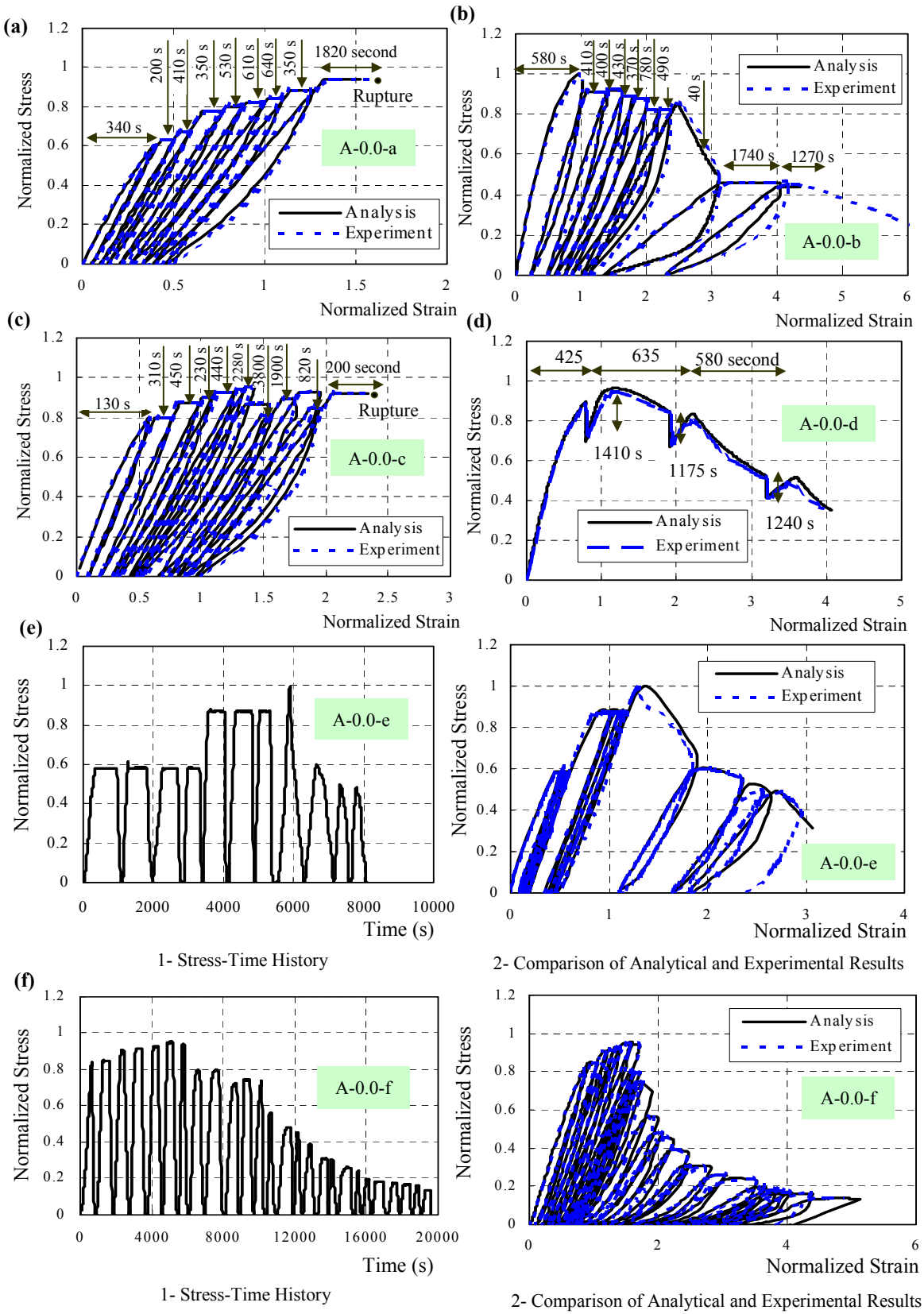

Fig. 14 Generic stress-strain paths and validation for unconfined concrete.

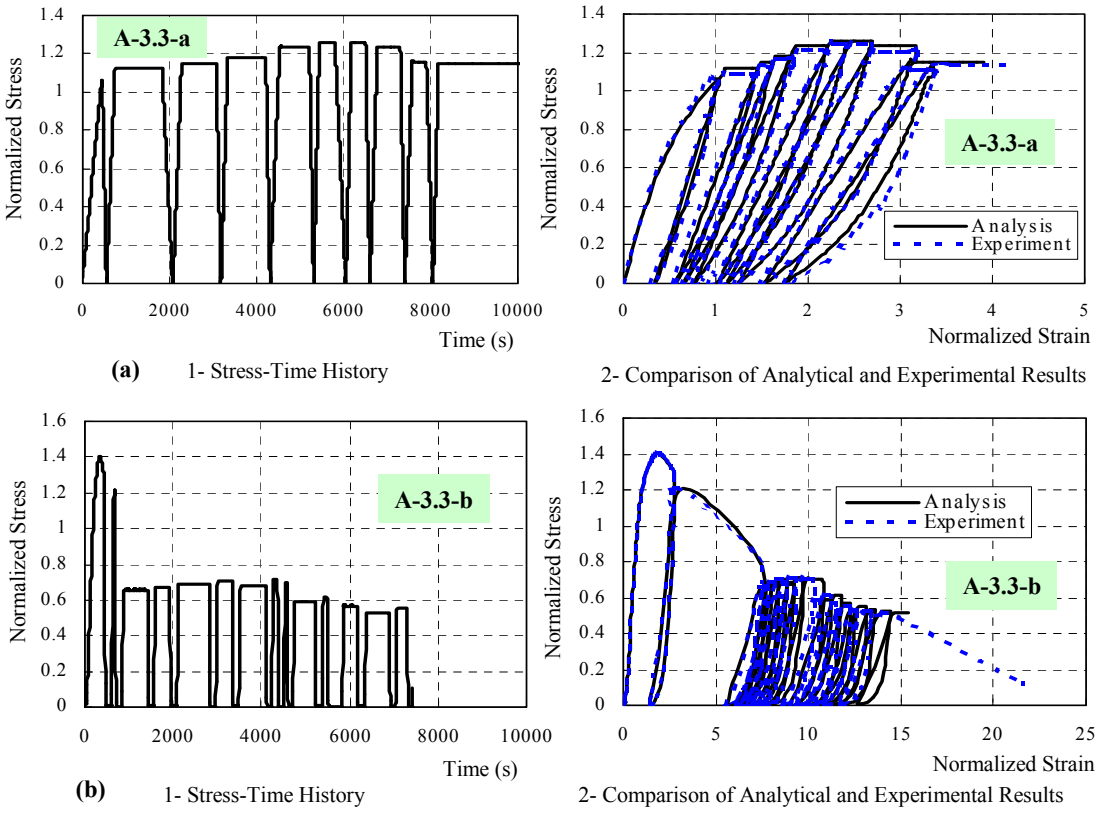

Fig. 15 Generic stress-strain paths and validation for confined concrete (3.3MPa).

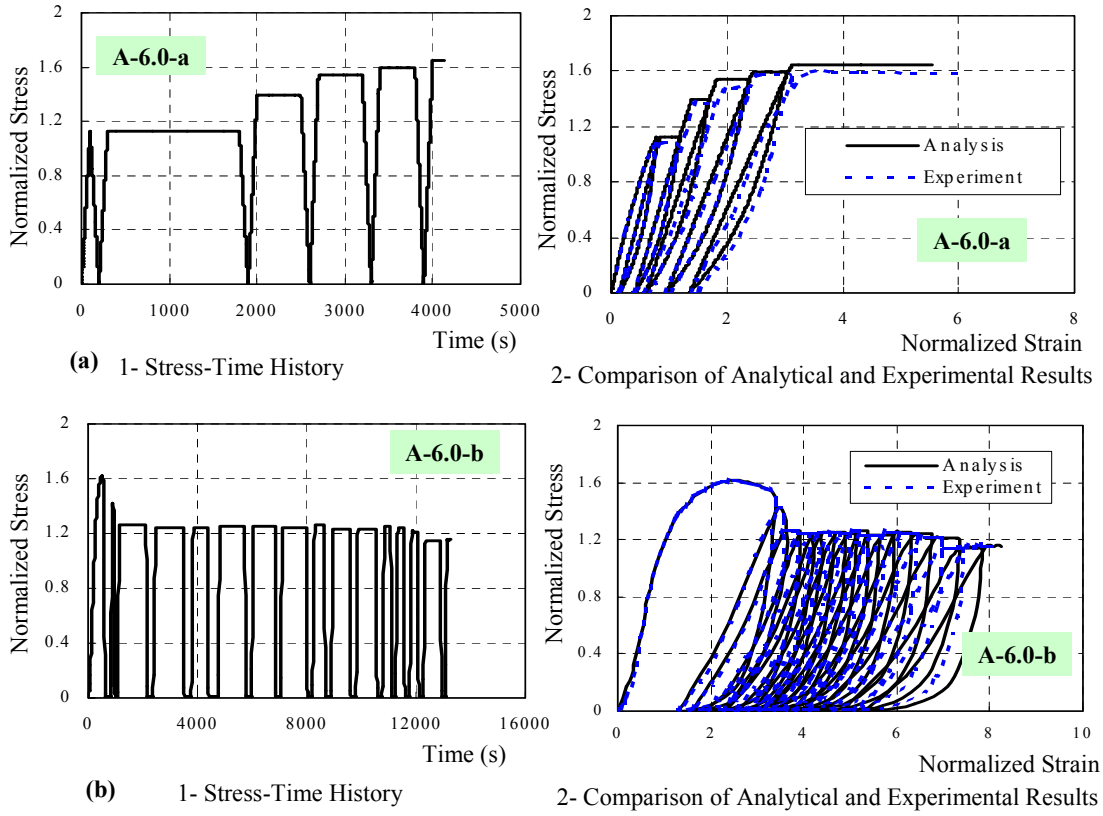

Fig. 16 Generic stress-strain paths and validation for confined concrete (6.0MPa).

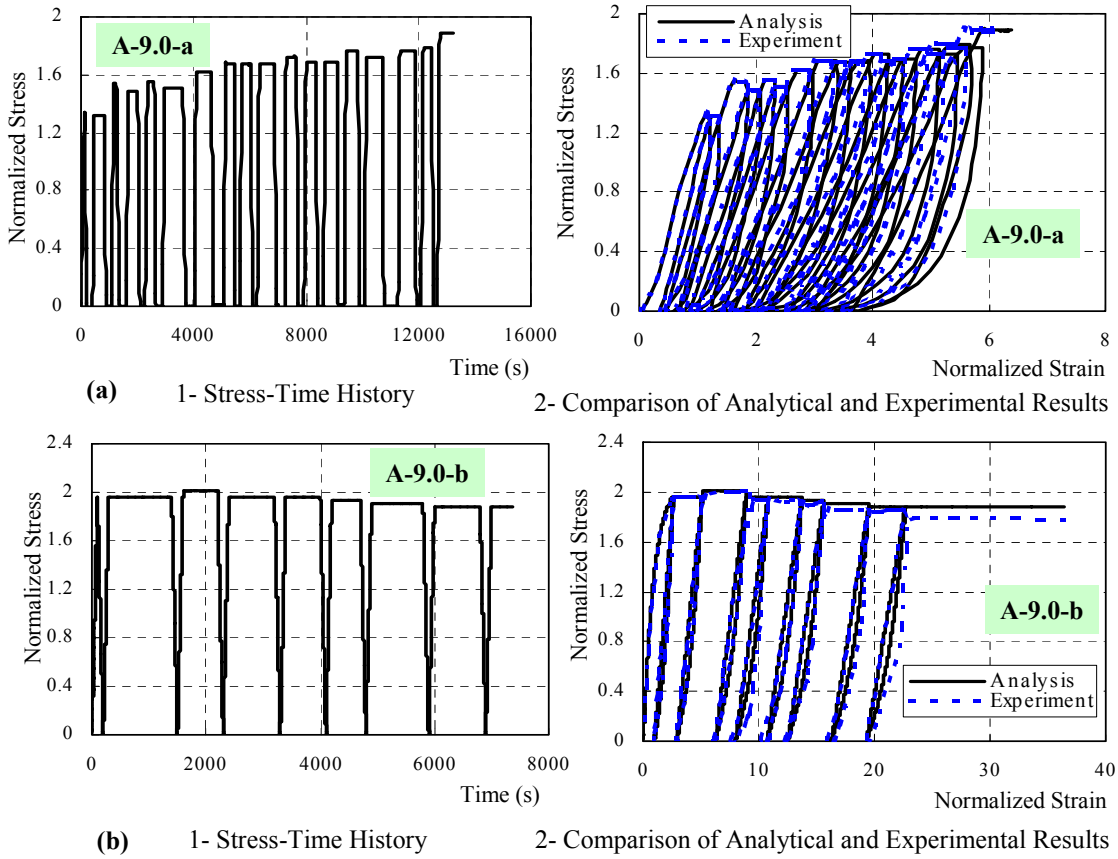

(a) 1- Stress-Time History 2- Comparison of Analytical and Experimental Results

(b) 1- Stress-Time History 2- Comparison of Analytical and Experimental Results

Fig. 17 Generic stress-strain paths and validation for confined concrete (9.0MPa).

5. Conclusions

Short-term time dependent constitutive modeling applicable to cyclic loads was proposed under pre- and post peak states for collapse analysis of concrete structures and the following conclusions were reached.

(1) The plastic and damaging rates of concrete could be experimentally extracted from the compression tests of cyclic loadings with and without confinement. Although creep, relaxation and their combined paths were actuated for taking out plastic flow rate and damaging, a unique relation between evolution of plastic damaging and state variables was found.

(2) The plastic evolution law was formulated in terms of updated elastic strain and the accumulated plasticity as demonstrated by the elasto-plastic and fracturing concept. The transient plastic flow rate of pre and post-peak regions was coherently expressed by using a single function.

(3) Similar to plasticity, the continuum-damaging rate was proposed as a function of updated elastic strain and the accumulated fracture parameter to indicate the reduction rate of unloading/reloading stiffness. Here, the time-dependent delayed fracture proportional to the static volume of concrete was newly conceptualized.

(4) Integrated modeling leads to total stress-strain relation by differential form and the modeling was verified in use of specimen-based experiments under uni-axial conditions. The effect of confinement was also validated for structural collapse analysis.

(5) The confining pressure mainly sets back damaging and results in stabilized stress carrying mechanics. The plastic flow is also controlled by confinement but its rate around the capacity is substantial. As a whole, time dependent compression softening is suppressed effectively.

Acknowledgments

The authors appreciate fruitful and valuable discussion with Dr. T. Ishida and Dr. T. Kishi of The University of Tokyo. This study was financially supported by Grant-in-Aid for Scientific Research (S) No.15106008.

References

Irawan, P. and Maekawa, K. (1994). "Three-dimensional analysis of strength and deformation of confined concrete columns." *Concrete Library of JSCE*, 24, 47-70.

Lettsrisakulrat, T., Watanabe, K., Matsuo, M. and Niwa, J. (2000). "Localization effects and fracture mechanism of concrete in compression." *Proceedings of JCI*, 22 (3), 145-150.

Maekawa, K., Pimanmas, A. and Okamura, H. (2003). "*Nonlinear Mechanics of Reinforced Concrete."* SPON Press.

Maekawa, K., Li, B. and Odagawa, M. (1984). "Influence of time and stress-strain path on deformation characteristic of concrete and its analytical model." Symposium on FEM Analysis of RC Structure, *JCI*, C5, 11-18. (In Japanese)

Mander, J. B, Priestley, M. J. N. and Park, R. (1988). "Theoretical stress-strain model for confined concrete." *Journal of the Structural Division*, ASCE, 114, 1804-1826.

Pallewatta, T. M., Irawan, P. and Maekawa, K. (1995). "Effectiveness of laterally arranged reinforcement on the confinement of core concrete." *Journal of Materials, Concrete structures and Pavements*, JSCE, V-28 (520), 297-308.

Richart, F. E., Brandtezaeg, A. and Brown, R. L. (1928). "A study of the failure of concrete under combined compressive stresses." Bulletin No. 1985, *University of Illinois, Urbana*, Nov. 1928.

Rusch, H. (1960). "Research towards a general flexural theory for structural concrete." *Journal of the ACI*, 57 (1), 1-27.

Scott, B. D., Park, R. and Priestley, M. J. N. (1982). "Stress-strain behavior of concrete confined by overlapping hoops at low and high strain rate." *Journal of the ACI*, 79 (1), 13-27.

Sheikh, S. A. (1982). "A comparative study of confinement models." *Journal of the ACI*, 79, 296-306.

Song, C., Maekawa, K. and Okumara H. (1991). "Time and path-dependent uniaxial constitutive model of concrete." *Journal of The Faculty of Engineering*, The University of Tokyo (B), XLI (1), 159-237.

Tabata, M. and Maekawa, K. (1984). "Prediction model for plasticity and failure of concrete based on time dependence." *Proceedings of JCI*, 6 (1), 269-272. (In Japanese)